

Behaviour of the Serre Equations in the Presence of Steep Gradients Revisited

J.P.A. Pitt^{a,*}, C. Zoppou^a, S.G. Roberts^a

^a*Mathematical Sciences Institute, Australian National University, Canberra, ACT 0200, Australia*

Abstract

Keywords: Serre equations, steep gradients, dam break

1. Introduction

2 The behaviour of steep gradients in a flow is important to shallow water modelling
3 both because there are problems in which steep gradients are present in the initial con-
4 ditions such as the propagation of a bore or the classical dam-break problem and also
5 because some problems develop steep gradients as they evolve such as shoaling waves
6 on a beach.

7 For the Serre equations there are no analytic solutions to problems containing steep
8 gradients. Although, expressions for the leading wave height and speed of an undular
9 bore were derived and verified for a range of different undular bores [1]. Therefore, we
10 resort to numerical methods to infer the structure of solutions to problems containing
11 steep gradients.

12 Unfortunately there are few examples in the literature which depict the behaviour
13 of numerical solutions to the Serre equations in the presence of steep gradients [1, 2,
14 3, 4]. These papers all present problems with discontinuous initial conditions [2] or a
15 smooth approximation to them [1, 3, 4]. Among these papers there are differences in
16 the structures of the numerical solutions implying different natures of the true solutions
17 of the Serre equations. Although, for the dam-break problem the analytic solution of
18 the shallow water wave equations has been demonstrated to capture the mean behaviour
19 of numerical solutions of the Serre equations despite smoothing of the initial conditions
20 [2, 3].

21 The aim of this paper is to investigate the effect of smoothing the initial condi-
22 tions on the structure of the numerical solutions of the Serre equations and assess the
23 usefulness of the analytic solution of the shallow water wave equations as well as the
24 Whitham modulation results of El et al. [1]. This is achieved by comparing the results

*Corresponding author

Email addresses: jordan.pitt@anu.edu.au (J.P.A. Pitt),
christopher.zoppou@anu.edu.au (C. Zoppou), stephen.roberts@anu.edu.au
(S.G. Roberts)

of five different numerical schemes. Three of which are the first, second and third-order methods presented by Zoppou et al. [5] where this first-order method is equivalent to the method of Le Métayer et al. [2]. The fourth method is a recreation of the second-order method used by El et al. [1]. Lastly the fifth method is a complete second-order finite difference approximation to the Serre equations.

These five methods were all used to solve a smooth approximation to the dam-break problem with the same heights as El et al. [1] and Le Métayer et al. [2] to investigate the differences among the structures of the published numerical solutions. It was found that the results of [2] were dominated by the diffusion of their first-order numerical method. While the results for the other papers were impacted by the smoothing of the initial conditions [1, 3, 4]. Through this process a new structure of the numerical solutions was found which has hitherto not been published. It was confirmed that the analytic solutions for the shallow water wave equations are a good guide for the mean behaviour of the numerical solutions. While the Whitham modulation results of El et al. [1] agree with our numerical solutions, and offer a better prediction of the speed of the bore than the shallow water wave equations.

The paper is organised as follows: The Serre equations are given, the numerical methods are described briefly with details left to the Appendix, then a smoothed approximation to the dam-break problem is presented and lastly the results of our numerical investigation into the behaviour of the Serre equations applied to the dam-break problem are presented.

2. Serre Equations

The Serre equations can be derived by integrating the full incompressible Euler equations over the water depth, see for example [6]. They can also be derived as an asymptotic expansion of the Euler equations, see for example [7]. Assuming a constant horizontal bed the one-dimensional Serre equations are [8]

$$\frac{\partial h}{\partial t} + \frac{\partial(uh)}{\partial x} = 0 \quad (1a)$$

and

$$\underbrace{\frac{\partial(uh)}{\partial t} + \frac{\partial}{\partial x} \left(u^2 h + \frac{gh^2}{2} \right)}_{\text{Shallow Water Wave Equations}} + \underbrace{\frac{\partial}{\partial x} \left(\frac{h^3}{3} \left[\frac{\partial u}{\partial x} \frac{\partial u}{\partial x} - u \frac{\partial^2 u}{\partial x^2} - \frac{\partial^2 u}{\partial x \partial t} \right] \right)}_{\text{Dispersion Terms}} = 0. \quad (1b)$$

Serre Equations

Where u is the horizontal velocity over the depth of water h , g is the acceleration due to gravity, x is the horizontal spatial variable and t is time.

2.1. Conservation

The Serre equations are conservation laws for mass (h) and momentum (uh) [6]. The Serre equations admit a Hamiltonian [9, 10]

$$\mathcal{H}(x, t) = \frac{1}{2} \left(hu^2 + \frac{h^3}{3} \left(\frac{\partial u}{\partial x} \right)^2 + gh^2 \right) \quad (2)$$

63 which represents the energy for the Serre equations and is conserved. The total amount
 64 of a quantity q in a system occurring on the interval $[a, b]$ is measured by

$$65 \quad C_q(t) = \int_a^b q(x, t) dx.$$

66 Conservation of a quantity q implies that $C_q(0) = C_q(t) \forall t$ provided the interval is
 67 fixed and the system is closed. Our numerical methods should have this conservation
 68 property for h , uh and \mathcal{H} .

70 3. Numerical Methods

71 Five numerical schemes are used to solve the Serre equations. The first (\mathcal{V}_1), sec-
 72 ond (\mathcal{V}_2) and third-order (\mathcal{V}_3) methods of [5], the method of El et al. [1] (\mathcal{E}) and a
 73 second-order finite difference method (\mathcal{G}). These methods all use a fixed grid in time
 74 and space, with subscripts denoting spatial indices and superscripts denoting time in-
 75 dices. Thus for a quantity q on our grid $q_i^n = q(x_i, t^n)$ with the grids uniform such that
 76 $\Delta x = x_i - x_{i-1} \forall i$ and $\Delta t = t^n - t^{n-1} \forall n$. A cell is a particularly useful unit of the finite
 77 volume method, the i th cell is the interval $[x_i - \Delta x/2, x_i + \Delta x/2]$ centered around x_i .

78 All methods are stable under the CFL condition [12] and have demonstrated the
 79 appropriate order of convergence for smooth problems [5]. Furthermore, \mathcal{V}_2 and \mathcal{V}_3
 80 have been validated against experimental data containing steep gradients [5]. For com-
 81 pleteness the two methods \mathcal{G} and \mathcal{E} which are not explicitly published are presented in
 82 the Appendix to allow for replication.

83 4. Smoothed Dam Break Problem

84 In the literature the dam-break problem is usually approximated by a smooth hy-
 85 perbolic tangent function [3, 4]. Such an approximation will be called a smoothed
 86 dam-break problem and will be defined by

$$87 \quad h(x, 0) = h_0 + \frac{h_1 - h_0}{2} \left(1 + \tanh\left(\frac{x_0 - x}{\alpha}\right) \right), \quad (3a)$$

$$88 \quad u(x, 0) = 0.0m/s. \quad (3b)$$

90 Where α measures the distance over which 46.117% of the smooth transition between
 91 the two heights of h_0 and h_1 centred around x_0 occurs. Figure 1 demonstrates the
 92 effect of varying α for the smoothed dam-break problem with $h_1 = 1.8m$, $h_0 = 1m$ and
 93 $x_0 = 500m$. These are the same h_0 and h_1 values as those of the dam-breaks presented
 94 by [1] and [2] and will be the values used in Sections 4 and 5.

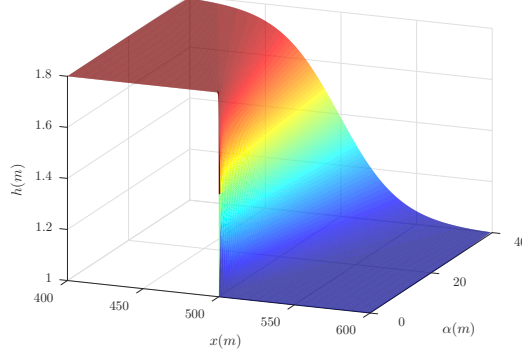


Figure 1: Initial conditions for the smooth dam-break problem with $h_0 = 1m$, $h_1 = 1.8m$ and $x_0 = 500m$ as α varies.

97 4.1. Measures and Comparisons

98 There are no analytic results for the Serre equations for either the discontinuous
 99 dam-break problem or its smoothed approximation. To assess the validity of our results
 100 we must resort to other comparisons such as measuring the error in the conservation
 101 of the conserved quantities and measuring the distance between numerical solutions as
 102 $\Delta x \rightarrow 0$. Le Métayer et al. [2] and Mitsotakis et al. [3] demonstrated that the analytic
 103 solution of the shallow water wave equations for the dam-break problem captures the
 104 mean behaviour of their numerical results. While El et al. [1] derived expressions
 105 for the leading wave height and speed of an undular bore in the Serre equations. We
 106 make use of all of these comparisons in Section 5 and so we present some relevant
 107 background for each here.

108 4.1.1. Conserved Quantities

109 The initial conditions of the smoothed dam-break (3) were integrated to get the
 110 following expressions for $C_h(0)$, $C_{uh}(0)$ and $C_H(0)$ provided x_0 is the midpoint of the
 111 spatial domain $[a, b]$ in which the smoothed dam-break occurs

$$112 \quad C_h(0) = \frac{h_1 + h_0}{2} (b - a), \\ 113$$

114

$$115 \quad C_{uh}(0) = 0$$

116 and

$$117 \quad C_H(0) = \frac{g}{4} \left(h_0^2 - h_1^2 + \alpha (h_1 - h_0)^2 \tanh \left(\frac{a - b}{2\alpha} \right) \right).$$

118

119 To calculate the total amount of a quantity q in our numerical solution we fit a
 120 quartic interpolant of the primitive variables h and u over a cell utilising neighbouring
 121 cells and then apply Gaussian quadrature with 3 points to get the total amount of q in a

124 cell and then sum this for all cells to get the total amount of q in our numerical solution
 125 at time t which we call $C^*_q(t)$. We then measure the error in conservation of a quantity
 126 q for a numerical method by

$$127 \quad C_1^q = \frac{|C_q(0) - C^*_q(t)|}{|C_q(0)|}. \quad (5)$$

128

129 Note that for uh the denominator is 0 and that there is a flux of momentum due to the
 130 unequal heights at both ends of the domain. To resolve these issues for uh we measure
 131 the error in the conservation of uh by

$$132 \quad C_1^{uh} = \left| C_{uh}(0) - C^*_{uh}(t) - \frac{gt}{2} (h(b)^2 - h(a)^2) \right|. \quad (6)$$

133

134 4.1.2. Distance between Numerical Results

135 By measuring the relative distance between numerical solutions we can assess
 136 whether our numerical solutions are converging as $\Delta x \rightarrow 0$. Rather than comparing
 137 all numerical results to one another we simplify by comparing all our numerical sol-
 138 utions to the one with the smallest Δx . For some quantity q we have a numerical
 139 approximation to it q' at the locations x_i and our numerical approximation to it with
 140 smallest Δx q^* at the locations x_j . By using grids such that for each i there is a $j^*(i)$
 141 such that $x_i = x_{j^*(i)}$ and summing the difference for each i

$$142 \quad L_1^q = \frac{\sum_i |q'_i - q^*_{j^*(i)}|}{\sum_i |q^*_{j^*(i)}|} \quad (7)$$

143

144 we can measure the relative distance between these numerical solutions on the grid x_i .

145 4.1.3. Shallow Water Wave Equation Analytic Solution for the Dam Break

146 For the discontinuous dam break problem the shallow water wave equations which
 147 are the Serre equations with dispersive terms neglected can be solved analytically. The
 148 analytic solution of the shallow water wave equations have been used as a comparative
 149 tool against numerical results in the literature [2, 3] as they appear to capture the mean
 150 behaviour of the numerical solutions.

151 An example of the analytic solution of the shallow water wave equations for the
 152 dam-break problem is presented in Figure 2 at $t = 30s$. Region I is the undisturbed
 153 water upstream of the dam-break at constant height (h_1) and velocity (0m/s) and region
 154 II is the rarefaction fan connecting regions I and III. Regions III and IV are the constant
 155 height (h_2) and constant velocity (u_2) state which are separated by $x_{u_2} = x_0 + u_2 t$ and
 156 region V is the undisturbed water downstream at constant height (h_0) and velocity
 157 (0m/s) separated from region IV by a shock which travels at velocity S_2 . Expressions
 158 for the unknown quantities h_2 , u_2 and S_2 in terms of h_0 and h_1 were given by Wu et al.
 159 [11]

$$160 \quad h_2 = \frac{h_0}{2} \left(\sqrt{1 + 8 \left(\frac{2h_2}{h_2 - h_0} \frac{\sqrt{gh_1} - \sqrt{gh_2}}{\sqrt{gh_0}} \right)^2} - 1 \right), \quad (8a)$$

161

162

163

$$u_2 = 2(\sqrt{gh_1} - \sqrt{gh_2}) \quad (8b)$$

165 and

166
167

$$S_2 = \frac{h_2 u_2}{h_2 - h_0}. \quad (8c)$$

168 From these values the location of the shock separating regions IV and V at time t is
 169 $x_{S_2}(t) = x_0 + S_2 t$. Applying (8) to our dam-break problem heights results in $h_2 =$
 170 $1.36898m$, $u_2 = 1.074975 m/s$ and $S_2 = 3.98835 m/s$ which are demonstrated in
 171 Figure 2.

172 *4.1.4. Whitham Modulation for Undular Bores of the Serre Equations*

173 Undular bores for the one dimensional Serre equations were analysed by [1] and an
 174 expression for the amplitude (A^+) and speed (S^+) of the leading wave of a bore shown
 175 in Figure 3 were given

$$\frac{\Delta}{(A^+ + 1)^{1/4}} - \left(\frac{3}{4 - \sqrt{A^+ + 1}} \right)^{21/10} \left(\frac{2}{1 + \sqrt{A^+ + 1}} \right)^{2/5} = 0 \quad (9a)$$

176 and

177
178

$$S^+ = \sqrt{g(A^+ + 1)} \quad (9b)$$

179 where $\Delta = h_b/h_0$, and h_b is the amplitude of the bore. From this we define $x_{S^+}(t) =$
 180 $x_0 + S^+ t$ which is the location of the leading wave at time t . The height of the bore
 181 created by the dam-break in (9) used by El et al. [1] was

$$h_b = \frac{1}{4} \left(\sqrt{\frac{h_1}{h_0}} + 1 \right)^2.$$

182 Thus for our dam-break problem $h_b = 1.37082 m$, $\Delta = 1.37082$, $A^+ = 1.73998 m$ and
 183 $S^+ = 4.13148 m/s$.

184 **5. Numerical Results**

185 We begin by looking into the effect of the initial steepness of the smoothed dam-
 186 break problem for different α values by observing what happens as $\Delta x \rightarrow 0$ and our
 187 numerical solutions better approximate the true solution of the Serre equations. To
 188 have the smallest error we use the highest order well validated model \mathcal{V}_3 in the fol-
 189 lowing investigation. From these results we then investigate numerical results for long
 190 time scales, how the shallow water wave equations analytic solution and El's Whitham
 191 modulation values compare to our results and then finally present some other findings
 192 about the behaviour of our numerical solutions.

193 All numerical methods used $\Delta t = 0.01\Delta x$ which is smaller than required by the
 194 CFL condition [12] which ensures stability of our schemes or the relation used by El
 195 et al. [1]. Δt was chosen to be smaller than necessary because for a final time of $t = 30s$
 196 making Δt small suppresses errors without excessively increasing the run-time of the
 197 experiments. \mathcal{V}_2 requires an input parameter to its slope limiter and this was chosen to
 be $\theta = 1.2$ [5].

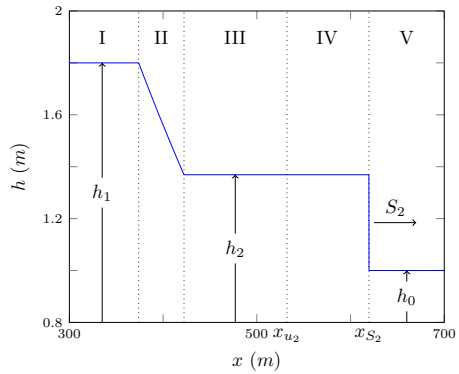


Figure 2: Analytic solution at $t = 30\text{s}$ of the shallow water wave equations for the dam-break problem with $h_0 = 1\text{m}$, $h_1 = 1.8\text{m}$ and $x_0 = 100\text{m}$.

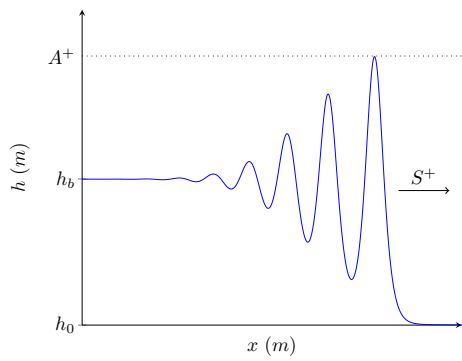


Figure 3: Demonstration of quantities obtained by Whitham modulation for undular bores of the Serre equations.

198 *5.1. Effect of alpha*

199 We observe that there are four different structures as $\Delta x \rightarrow 0$ depending on the
200 α and the numerical method. The four structures are identified by the nature of the
201 solutions around x_{u_2} when Δx is small and they correspond to different structures in the
202 numerical solutions presented in the literature. For brevity the only given examples of
203 these structures will be the solutions of \mathcal{V}_3 at $t = 30s$ on the interval $x \in [0m, 1000m]$
204 although they all also occurred for the numerical results of \mathcal{E} , \mathcal{G} and \mathcal{V}_2 using the same
205 α and $\Delta x = 10/2^{10}m$. All of the numerical methods presented use Dirichlet boundary
206 conditions with $u = 0m/s$ at both boundaries and $h = 1.8m$ on the left and $h = 1m$ on
207 the right.

208 *5.1.1. Non-oscillatory Structure*

209 The first structure which will be referred to as the non-oscillatory structure is the
210 result of a large α . When α is large enough for the smoothed dam-break problem the
211 fluid to the left of x_0 flows to fill the right side, but since α is large the front of this flow
212 is not steep enough to generate undulations over short time spans. Eventually the front
213 of this flow steepens due to non-linearity and undulations develop there.

214 This structure is not present in the literature as no authors chose large enough α . An
215 example of this structure can be seen in Figure 4 for $\alpha = 40m$ using \mathcal{V}_3 , this structure
216 was also observed for \mathcal{V}_1 's numerical solutions. Because this is a very smooth problem
217 we observe that all numerical results are visually identical for all $\Delta x < 10/2^4m$. We
218 note that \mathcal{V}_3 's numerical solution has $h(x_{u_2}) > h_2$ and because no undulations are
219 present the results of El et al. [1] are not applicable to these solutions.

220 From Table 1 it can be seen that the numerical solutions of \mathcal{V}_3 conserve the con-
221 served quantities very well for this particular α for both Δx 's, although the smaller
222 Δx 's numerical results are superior. C_1^{uh} is the worst performing of the measures be-
223 cause the smoothed dam-break has such a large transition width that $h(0m) \neq 1.8m$
224 and $h(1000m) \neq 1m$ causing small flows at the boundaries meaning the system is not
225 closed.

226 These measures verify that we are converging as $\Delta x \rightarrow 0$ and our solutions are
227 relatively conservative as the errors for the highest resolution results except for C_1^{uh}
228 are all at round-off error for each cells value as there are 100,000 cells. Therefore the
229 numerical result in Figure 4 is an accurate representation of the behaviour of the Serre
230 equations when α is sufficiently large and in particular $\alpha = 40m$.

231 *5.1.2. Flat Structure*

232 The second structure will be referred to as the flat structure due to the presence
233 of a constant height around x_{u_2} , this is the most common structure observed in the
234 literature [2, 3, 4]. This structure consists of oscillations in regions III and IV which
235 are separated by a constant height state around x_{u_2} . An example of this structure can be
236 seen in the numerical solutions presented in Figure 5 when $\alpha = 2m$, this structure was
237 also observed for \mathcal{V}_1 's solutions.

238 As Δx decreases the numerical solutions converge so that by $\Delta x = 10/2^8m$ the
239 solutions for higher Δx are visually identical. There is also good agreement between
240 the peak amplitude in region IV (A) and A^+ as well as $h(x_{u_2})$ and h_2 . Although as

α (m)	Δx (m)	C_1^h	C_1^{uh}	C_1^H	L_1^h	L_1^u
40	$10/2^4$	2.0×10^{-11}	1.8×10^{-6}	1.2×10^{-8}	1.7×10^{-7}	2.9×10^{-6}
40	$10/2^{10}$	1.8×10^{-11}	2.2×10^{-8}	3.6×10^{-11}	2.5×10^{-11}	6.5×10^{-11}
2	$10/2^4$	4.9×10^{-14}	5.1×10^{-3}	8.7×10^{-4}	5.0×10^{-3}	6.8×10^{-2}
2	$10/2^{10}$	4.0×10^{-12}	5.0×10^{-9}	2.0×10^{-8}	1.8×10^{-7}	2.3×10^{-6}
0.4	$10/2^4$	9×10^{-14}	4.8×10^{-3}	1.0×10^{-3}	$6.8 \times 10^{-3} \dagger$	$9.9 \times 10^{-2} \dagger$
0.4	$10/2^{10}$	3.9×10^{-12}	5.0×10^{-9}	2.0×10^{-8}	$3.6 \times 10^{-7} \dagger$	$5.0 \times 10^{-6} \dagger$
0.1	$10/2^4$	7.6×10^{-14}	4.8×10^{-3}	1.0×10^{-3}	$7.0 \times 10^{-3} \dagger$	$1.0 \times 10^{-1} \dagger$
0.1	$10/2^{10}$	3.9×10^{-12}	4.6×10^{-8}	7.6×10^{-7}	$5.0 \times 10^{-7} \dagger$	$6.4 \times 10^{-6} \dagger$

Table 1: All errors in conservation C_1^q (6) for the conserved quantities and relative distances L_1^q (7) of the primitive variables for numerical solutions of \mathcal{V}_3 . L_1^q uses the numerical solution with $\Delta x = 10/2^{11}m$ as the high resolution basis of comparison and \dagger indicates where the interval $[520m, 540m]$ has been omitted from the comparison.

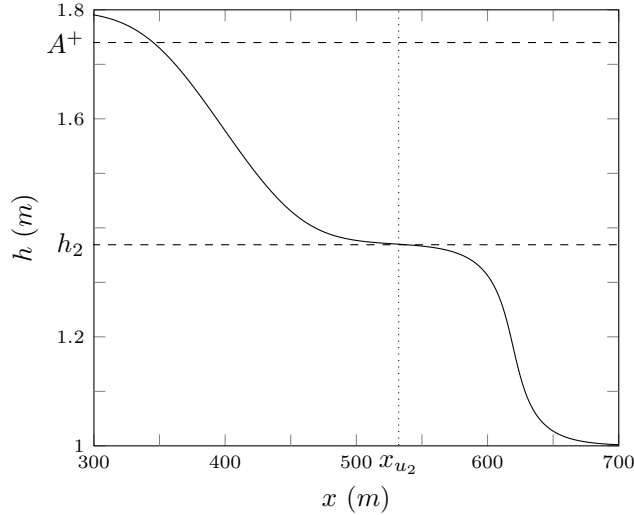


Figure 4: Numerical results of \mathcal{V}_3 at $t = 30s$ for the smooth dam-break problem with $\alpha = 40m$ for $\Delta x = 10/2^4 m$ (—).

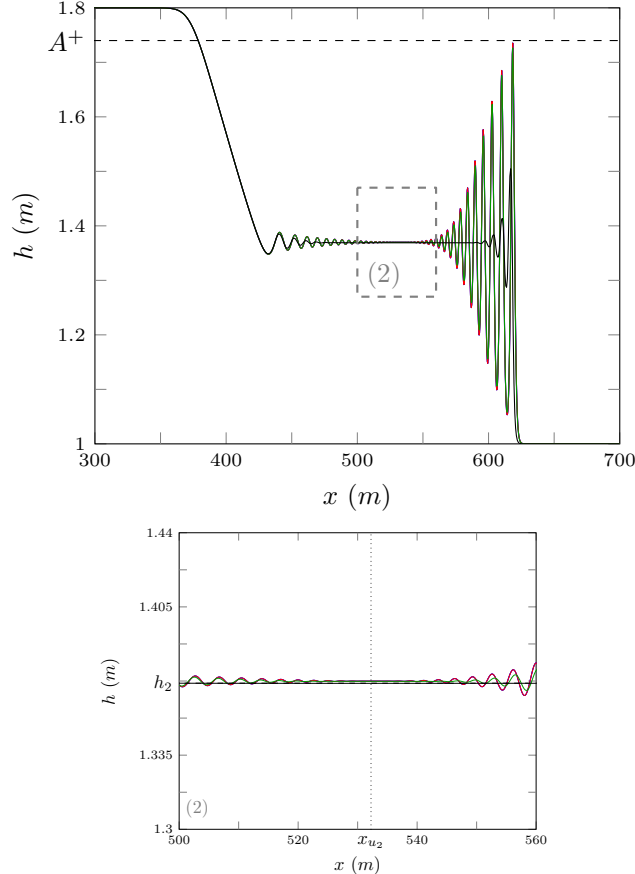


Figure 5: Numerical results of \mathcal{V}_3 at $t = 30s$ for the smooth dam-break problem with $\alpha = 2m$ for $\Delta x = 10/2^{10}m$ (blue), $10/2^8m$ (red), $10/2^6m$ (green) and $10/2^4m$ (black).

241 Δx is decreased in the simulations we observe $h(x_{u_2}) > h_2$. Since this method is well
 242 validated for smooth problems and a small Δx has been chosen this suggests that the
 243 mean bore heights in regions III and IV from a dam-break may differ slightly between
 244 the shallow water wave equations and the Serre equations. These solutions replicate
 245 the structure of the numerical solutions of Mitsotakis et al. [4] who use the same α but
 246 different h_0 and h_1 .

247 Table 1 demonstrates good conservation of the conserved quantities for our numeri-
 248 cal solution with $\Delta x = 10/2^{10}m$, although only the errors in conservation of h are at
 249 the size of round-off errors. The L_1 measures demonstrate that our solutions are very
 250 close to the numerical solution with $\Delta x = 10/2^{11}m$.

251 These results demonstrate that the numerical solutions in Figure 5 are an accurate
 252 representation of the nature of the Serre equations provided α and Δx are appropriate
 253 supporting the numerical solutions of [4] who used the same α but different h_0 and h_1
 254 values.

255 **5.1.3. Node Structure**

256 The third structure will be referred to as the node structure and it is was observed by
257 [1]. The node structures main feature is that the oscillations in region III and IV decay
258 and appear to meet at x_{u_2} as can be seen in Figure 6 when $\alpha = 0.4m$. Unfortunately
259 these numerical solutions are not visually identical for the higher resolutions as they
260 were in the flat structure example. However, the numerical solutions are getting closer
261 to one another and convergence is expected for the smaller Δx because the problem
262 is still smooth. In these results A^+ is a good estimator for A and the oscillations in
263 regions III and IV appear to be around h_2 . This structure was observed by [1] for \mathcal{E}
264 and indeed we have replicated it. This structure was not observed in \mathcal{V}_1 's solutions up
265 to $\Delta x = 10/2^{10}m$ with $\alpha = 0.001m$ as \mathcal{V}_1 introduces numerical diffusion that severely
266 dampen oscillations. This explains why the numerical solutions of Le Métayer et al. [2]
267 using \mathcal{V}_1 have a different structure to those of El et al. [1]. It was found that an α of at
268 least $0.4m$ is required to recover the node structure which explains why Mitsotakis et al.
269 [3] and Mitsotakis et al. [4] using α 's of $2m$ and $1m$ respectively could not reproduce
270 the structure in the numerical solutions of El et al. [1].

271 Figure 6 demonstrates that our numerical solutions have not converged, however
272 this is only in the area around x_{u_2} . This indicates that our solutions away from x_{u_2} are
273 consistent, in particular our results for A . The larger distance between numerical solu-
274 tions means we cannot get a meaningful measure of L_1 for the whole domain. However,
275 by omitting an interval around x_{u_2} such as $[520m, 540m]$ a meaningful measure of L_1
276 can be calculated, this modified L_1 is presented in Table 1. These modified L_1 's demon-
277 strate that our solutions are close to one another and have converged away from x_{u_2} , so
278 that increasing the grid resolution further would only cause a significant change in the
279 numerical solutions around x_{u_2} . Table 1 shows that for $\Delta x = 10/2^{10}m$ our conserved
280 quantities are very well conserved by our numerical solution.

281 These results suggest that although we have not yet fully converged these numerical
282 solutions are close to reasonable solutions of the Serre equations for the smoothed dam-
283 break problem for an appropriate α value supporting the structure of the numerical
284 solutions presented by El et al. [1].

285 **5.1.4. Growth Structure**

286 The fourth structure will be referred to as the growth structure due to the oscillations
287 in regions III and IV growing around x_{u_2} as can be seen in Figure 7 for $\alpha = 0.1m$. This
288 structure could not be replicated for \mathcal{V}_1 and has hitherto not been published.

289 Figure 7 shows that the disagreement in the numerical results is concentrated around
290 x_{u_2} . A is again predicted by A^+ well and the oscillations in regions III and IV are around
291 h_2 . The different resolution numerical results are getting closer to one another, but the
292 sudden change in structure around x_{u_2} makes it difficult to assert that large growths
293 in amplitude are not possible around x_{u_2} as we take Δx smaller. However, for nu-
294 matical solutions with $\alpha = 0.001m$ and $\Delta x = 10/2^{11}m$ these oscillations around x_{u_2}
295 stayed within the interval $[1.455m, 1.3m]$. The number of oscillations is the same for
296 $\Delta x = 10/2^{10}m$ in Figures 6 and 7 with different α values so that the change in structure
297 is a result of the difference in amplitudes of the oscillations and not an increase in their
298 number.

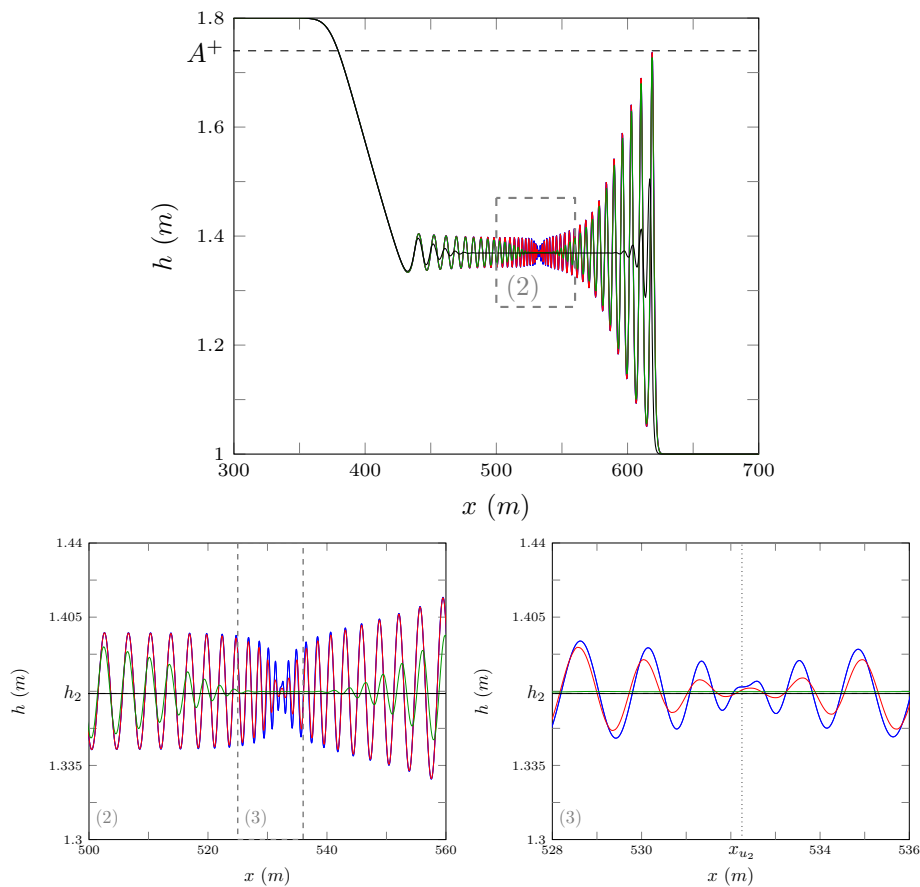


Figure 6: Numerical results of \mathcal{V}_3 at $t = 30s$ for the smooth dam-break problem with $\alpha = 0.4m$ for $\Delta x = 10/2^{10}m$ (—), $10/2^8m$ (—), $10/2^6m$ (—) and $10/2^4m$ (—).

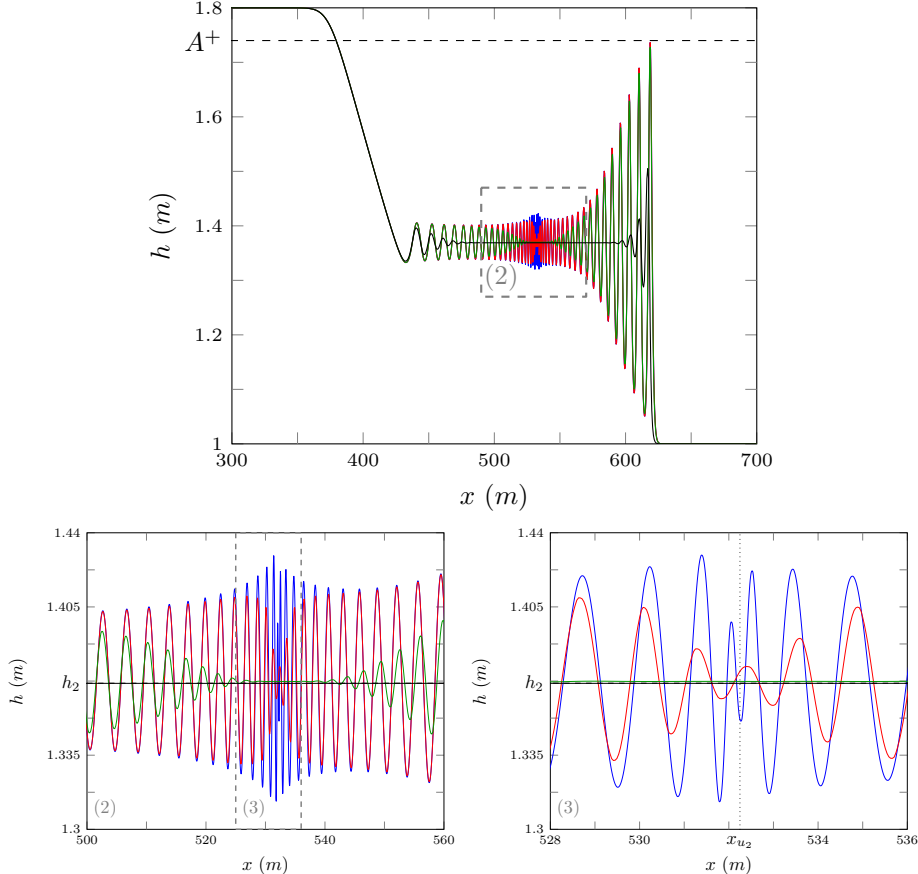


Figure 7: Numerical results of \mathcal{V}_3 at $t = 30s$ for the smooth dam-break problem with $\alpha = 0.1m$ for $\Delta x = 10/2^{10}m$ (—), $10/2^8m$ (—), $10/2^6m$ (—) and $10/2^4m$ (—).

The interval $[520m, 540m]$ has been omitted from L_1 in Table 1 due to the lack of convergence in this region. The L_1 measures for the numerical solution with $\alpha = 0.1m$ and $\Delta x = 10/2^{10}m$ are very close but slightly larger than those for the node structure, confirming that our numerical solutions are correctly capturing the behaviour of the Serre equations for this problem away from x_{u_2} . The errors in conservation are small, and in particular our conservation of h is as good as those in node and flat structures. The errors in conservation of uh and \mathcal{H} however are larger than the previous structures examples by a factor of 10.

Since this our numerical results have poorer convergence and conservation and cannot be found in the literature, we resort to using many different methods to support the numerical solutions of \mathcal{V}_3 . To remove the possibility that some effect from the reformulation of the Serre equations or the elliptic solver of the \mathcal{V}_i methods are the cause we use make use of \mathcal{G} and \mathcal{E} . \mathcal{G} , \mathcal{E} , \mathcal{V}_1 and \mathcal{V}_3 are applied to the same initial conditions with the same grid resolutions as above and the results were plotted in Figure

313 8. \mathcal{V}_2 has been omitted from this figure for clarity because its solution is very close to
314 \mathcal{V}_3 .

315 The first observation is that \mathcal{V}_1 has not recovered a growth structure. This is be-
316 cause \mathcal{V}_1 is very diffusive [5], dampening these oscillations. To resolve this structure
317 for \mathcal{V}_1 would require restrictively small Δx and as such this has not been observed in
318 the simulations. Secondly, all high-order methods recover this growth structure and
319 disagree only in the region around x_{u_2} . The absence of the growth structure in the
320 findings of El et al. [1] is the result of smoothing of the initial conditions [13].

321 Generally dispersive methods overestimate the size and number of oscillations of
322 the true solution while diffusive methods underestimate the size and number of oscil-
323 lations in the true solution. Since \mathcal{V}_3 is diffusive as can be seen in Figure 7 and \mathcal{G}
324 is dispersive the true analytic solution should exist between \mathcal{V}_3 and \mathcal{G} . As \mathcal{G} and \mathcal{V}_3
325 have the same number of oscillations we expect that the true solution will have the
326 same number of oscillations with different amplitudes. \mathcal{G} has very similar numerical
327 solutions to \mathcal{V}_2 and \mathcal{V}_3 which are preferred by the authors due to their robustness and
328 superior conservation of quantities.

329 These results demonstrate that while our numerical results have not converged as
330 $\Delta x \rightarrow 0$ the agreement of all the discussed methods of sufficiently high order indicates
331 that these results are representative of actual solutions of the smoothed dam-break prob-
332 lem with low α for the Serre equations. This is the same structure that we observe for
333 \mathcal{V}_2 and \mathcal{V}_3 with the same Δx and Δt for the dam-break.

334 5.2. Long time

335 To assess long term behaviour of the numerical solutions a smoothed dam-break
336 was solved by \mathcal{V}_3 with the same parameters on a larger domain $x \in [-900m, 1800m]$
337 for a longer time $t \in [0, 300s]$. The results of \mathcal{V}_3 with $\alpha = 0.1m$ and $\Delta x = 10/2^9m$ and
338 $10/2^8m$ at $t = 300s$ are presented in Figure 9. For this problem these parameters result
339 in the growth structure, however after sufficient time this growth structure has decayed
340 back into a flat structure although there are still small oscillations present in the middle
341 region.

342 To track the decaying of the oscillations for \mathcal{V}_3 's solution around x_{u_2} a snapshot
343 of the area around x_{u_2} has been plotted for different times in Figure 10. It can be
344 seen that at $t = 30s$ the solution exhibits the growth structure but as time progresses
345 the region around x_{u_2} has decayed into the node structure by $t = 100s$ and then into
346 the flat structure observed at $t = 200s$ and $t = 300s$. This is most likely due to the
347 accumulation of diffusive errors of the numerical method with Figure 9 demonstrating
348 that over this time span we are not close to convergence of the numerical results.

349 5.3. Shallow water wave equation comparison

350 The shallow water wave equations have been used as a guide for the mean be-
351 haviour of the solution of the Serre equations for the dam-break problem in the litera-
352 ture [2, 3]. We assess their applicability by plotting $h - h_2$ and $u - u_2$ for the smoothed
353 dam-break problem with $\alpha = 0.1m$ and $\Delta x = 10/2^9m$ in Figure 11 for $t = 30s$ and
354 Figure 12 for $t = 300s$.

355 From these results it can be seen that over short time spans both h_2 and u_2 are good
356 approximations to the mean behaviour of the fluid with both plots oscillating around 0.

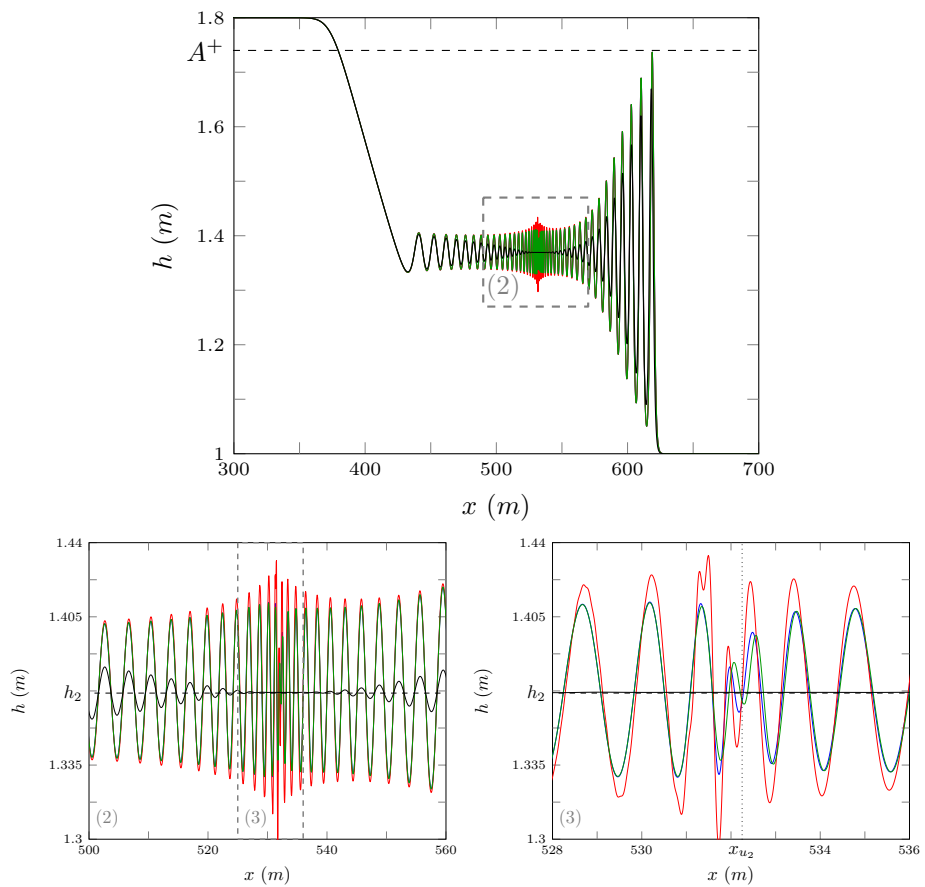


Figure 8: Numerical results for the smooth dam-break problem with $\alpha = 0.1m$ and $\Delta x = 10/2^{10}m$ for \mathcal{G} (—), \mathcal{E} (—), \mathcal{V}_3 (—), and \mathcal{V}_1 (—).

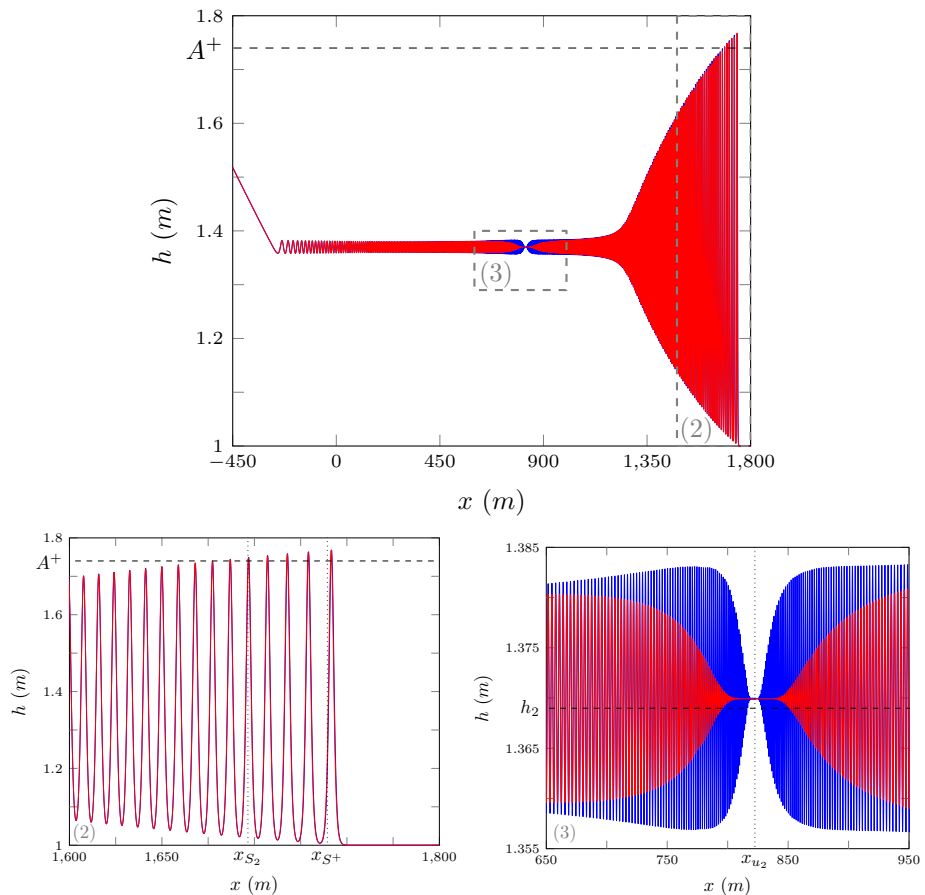


Figure 9: Numerical solution of smooth dam-break problem at $t = 300s$ by \mathcal{V}_3 with $\alpha = 0.1m$ for $\Delta x = 10/2^9 m$ (blue) and $10/2^8 m$ (red).

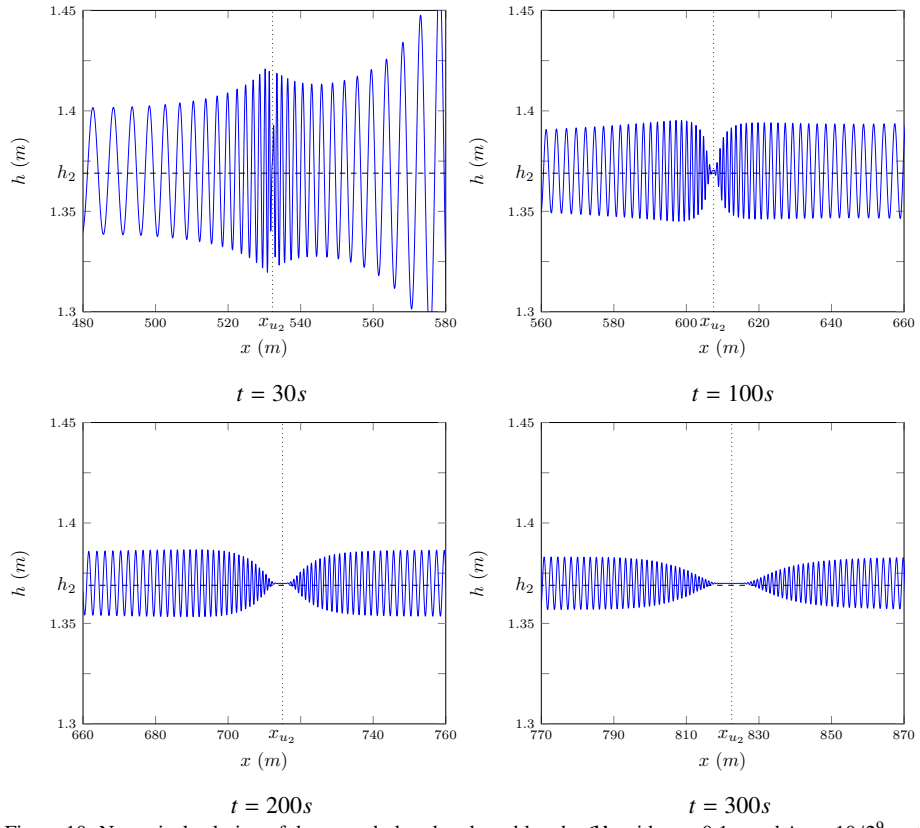


Figure 10: Numerical solution of the smooth dam-break problem by \mathcal{V}_3 with $\alpha = 0.1m$ and $\Delta x = 10/2^9 m$ at various times.

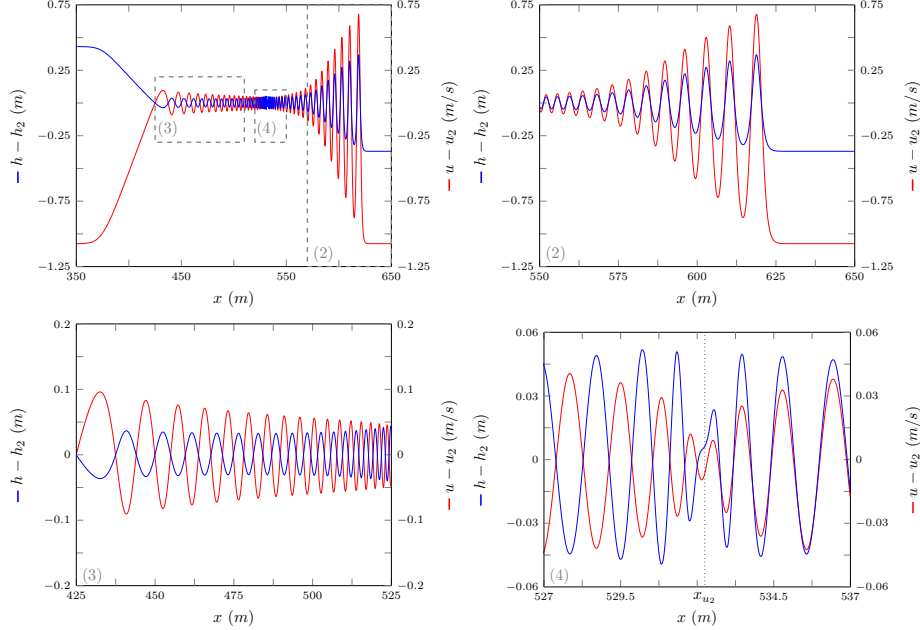


Figure 11: $h - h_2$ (blue) and $u - u_2$ (red) for numerical solution of the smooth dam-break by \mathcal{V}_3 with $\alpha = 0.1m$ and $\Delta x = 10/2^9 m$ at $t = 30s$ as in Figure 7.

357 However after sufficient time the mean velocity and height of the bore have diverged
 358 slightly from the shallow water wave equation values h_2 and u_2 . With h_2 being an
 359 underestimate and u_2 being an overestimate. While Figure 9 demonstrates that S_2 is a
 360 worse approximation than h_2 and u_2 .

361 5.4. Contact discontinuity

362 El et al. [1] noted the presence of a ‘degenerate contact discontinuity’ which travels
 363 at the mean velocity in the bore and has zero amplitude. The structure around this point
 364 is the central difference between the different structures.

365 The contact discontinuity is the location of the node in the node structure [1] and the
 366 growth of the oscillations in the growth structure, we have demonstrated that this is at
 367 about x_{u_2} as can be seen in Figures 6 and 7. Figures 11 and 12 show a more fundamental
 368 property of the contact discontinuity, that it is the transition between when h and u are
 369 anti-phase to the left and when h and u are in-phase to the right.

370 By inspecting the phase velocity for the linearised Serre equations

$$371 \quad 372 \quad v_p = u \pm \sqrt{gh} \sqrt{\frac{3}{h^2 k^2 + 3}} \quad (10)$$

373 with wave number k , it can be seen that as $k \rightarrow \infty$ then $v_p \rightarrow u$ and as $k \rightarrow 0$
 374 then $v_p \rightarrow u \pm \sqrt{gh}$. Therefore when u and h are anti-phase this corresponds to the
 375 negative branch of the phase velocity $u - \sqrt{gh} \sqrt{3/(h^2 k^2 + 3)}$ and when u and h are
 376 in-phase this corresponds to the positive branch $u + \sqrt{gh} \sqrt{3/(h^2 k^2 + 3)}$. So that the

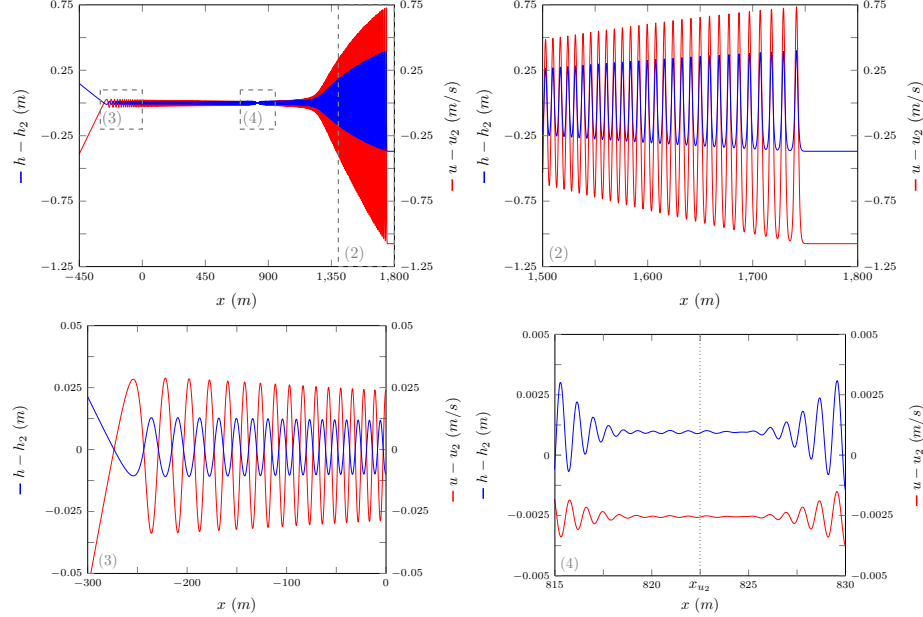


Figure 12: $h - h_2$ (blue) and $u - u_2$ (red) for numerical solution of the smooth dam-break by \mathcal{V}_3 with $\alpha = 0.1m$ and $\Delta x = 10/2^9 m$ at $t = 300s$ as in Figure 9.

377 contact discontinuity is the location of the highest wave numbers and it travels at speed
 378 u which would be the mean velocity inside the bore. This explains why the structure
 379 of the numerical solutions around the contact discontinuity is sensitive to smoothing of
 380 the initial conditions and diffusion of the method.

381 A range of different mean bore speeds where modelled with smoothed dam-break
 382 problems by fixing $h_0 = 1m$ and varying h_1 to allow for different aspect ratios and thus
 383 different bore speeds. The results are plotted in Figure 13 which shows that the contact
 384 discontinuity travels at a speed close to u_2 for a range of mean bore speeds.

385 These results demonstrate that while h_2 and u_2 are not exactly the mean behaviour
 386 of the bore for the Serre equations the two are highly correlated across a range of
 387 different smoothed dam-break problems and so the analytic solutions of the shallow
 388 water wave equations are a good guide for the mean behaviour of the Serre equations.

389 5.5. Whitham modulation comparison

390 The expressions for the leading wave amplitude A^+ and speed S^+ obtained by [1]
 391 are asymptotic results and so we are interested in how our numerical results behave
 392 over time. Thus for the dam-break problem in Figure 9 the peak amplitude in region
 393 IV (A) was plotted over time in Figure 14. It can be seen that A approaches a value larger
 394 than A^+ over time. We find that as $\alpha \rightarrow 0$ and $\Delta x \rightarrow 0$ A converges away from A^+ in
 395 this time scale for this aspect ratio. Thus it appears that the true solution of the dam-
 396 break for the Serre equations has an amplitude in region IV slightly above A^+ . This
 397 is not inconsistent with the results of [1] as their scale comparing A^+ to A is too large

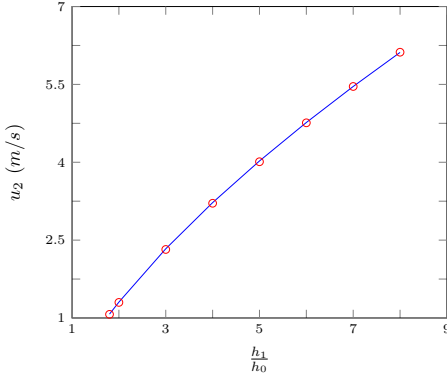


Figure 13: u_2 (—) and speed of the contact discontinuity (○) for numerical solutions of smoothed dam-break problems with different aspect ratios (h_1/h_0) by \mathcal{V}_3 where $\alpha = 0.1\text{m}$ and $\Delta x = 10/2^9\text{m}$ at $t = 100\text{s}$.

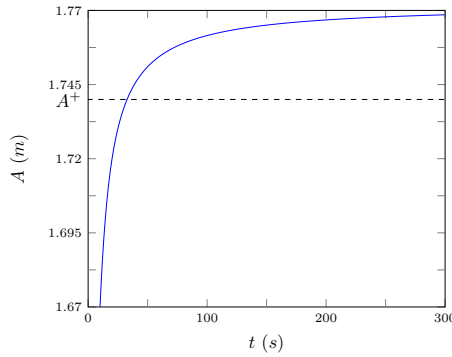


Figure 14: Leading wave height plotted over time for the numerical solution of the smooth dam-break problem by \mathcal{V}_3 with $\alpha = 0.1\text{m}$ for $\Delta x = 10/2^9\text{m}$ (—) as in Figure 9.

398 to see such a small difference. From Figure 9 it can be seen that while S^+ does not
399 precisely predict the bore speed it is a better prediction than S_2 .

400 These results together with those of El et al. [1] demonstrate that A and A^+ are
401 highly correlated across a range of different smoothed dam-break problems, but for a
402 given problem these two are not precisely equal for our numerical results.

403 6. Conclusions

404 Utilising two finite difference methods of second-order and three finite difference-
405 volume hybrid methods of various orders an investigation into the smoothed dam-break
406 problem with varying steepness was performed. Four different structures of the numer-
407 ical solutions were uncovered with the general trend being that an increase in steepness
408 increases the size and number of oscillations in the solution. This study explains the
409 different numerical results in literature involving the solution of the Serre equations
410 applied to the smoothed dam-break problem and also uncovers a new result. We find
411 that while the analytic solution of the shallow water wave equations for the dam-break

412 problem is a good guide to the mean behaviour of the Serre equations the speed and
413 height of the bores do not match up precisely. While the Whitham modulation results
414 for the Serre equations give better predictions than the shallow water wave equations
415 analytic solution it was found that they also do not line up with our numerical results
416 precisely. Lastly, it was demonstrated that the contact discontinuity corresponds to high
417 wave numbers and thus travels at the mean velocity inside the bore.

- 418 [1] G. El, R. H. J. Grimshaw, N. F. Smyth, Unsteady undular bores in fully nonlinear
419 shallow-water theory, *Physics of Fluids* 18 (027104).
- 420 [2] O. Le Métayer, S. Gavrilyuk, S. Hank, A numerical scheme for the GreenNaghdi
421 model, *Journal of Computational Physics* 229 (6) (2010) 2034–2045.
- 422 [3] D. Mitsotakis, B. Ilan, D. Dutykh, On the Galerkin/Finite-Element Method for
423 the Serre Equations, *Journal of Scientific Computing* 61 (1) (2014) 166–195.
- 424 [4] D. Mitsotakis, D. Dutykh, J. Carter, On the nonlinear dynamics of the traveling-
425 wave solutions of the Serre system, *Wave Motion* 70 (1) (2017) 166–182.
- 426 [5] C. Zoppou, J. Pitt, S. Roberts, Numerical Solution of the Fully Non-linear Weakly
427 Dispersive Serre Equations for Steep Gradient Flows, *Applied Mathematical
428 Modelling* 00 (00) (2017) 00–00.
- 429 [6] C. H. Su, C. S. Gardner, Korteweg-de Vries equation and generalisations. III.
430 Derivation of the Korteweg-de Vries equation and Burgers equation, *Journal of
431 Mathematical Physics* 10 (3) (1969) 536–539.
- 432 [7] D. Lannes, P. Bonneton, Derivation of asymptotic two-dimensional time-
433 dependent equations for surface water wave propagation, *Physics of Fluids* 21 (1)
434 (2009) 16601–16610.
- 435 [8] M. Li, P. Guyenne, F. Li, L. Xu, High order well-balanced CDG-FE methods
436 for shallow water waves by a Green-Naghdi model, *Journal of Computational
437 Physics* 257 (2014) 169–192.
- 438 [9] Y. A. Li, Hamiltonian Structure and Linear Stability of Solitary Waves of the
439 Green-Naghdi Equations, *Journal of Nonlinear Mathematical Physics* 9 (2002)
440 99–105.
- 441 [10] A. E. Green, P. M. Naghdi, A derivation of equations for wave propagation in
442 water of variable depth, *Journal of Fluid Mechanics* 78 (2) (1976) 237–246.
- 443 [11] C. Wu, G. Huang, Y. Zheng, Theoretical solution of dam-break shock wave, *Jour-
444 nal of Hydraulic Engineering* 125 (11) (1999) 1210–1215.
- 445 [12] A. A. Harten, High resolution schemes for hyperbolic conservation laws, *Journal
446 of Computational Physics* 49 (3) (1983) 357–393.
- 447 [13] G. El, M. Hoefer, Dispersive shock waves and modulation theory, *Physica D:
448 Nonlinear Phenomena* 333 (2016) 11–65.

449 **Appendix A.**

450 \mathcal{E} and \mathcal{G} use the centred second-order finite difference approximation to the con-
 451 servation of momentum equation (1b) denoted as \mathcal{G}_u . For the conservation of mass
 452 equation (1a) \mathcal{E} uses the two step Lax-Wendroff method denoted as \mathcal{E}_h while \mathcal{G} uses a
 453 centred second-order finite difference approximation denoted as \mathcal{G}_h .

454 *Appendix A.1. \mathcal{G}_u for Conservation of Momentum Equation*

455 The finite difference approximation to (1b) on our grid is

$$456 \quad h_i^n u_i^{n+1} - (h_i^n)^2 \left(\frac{u_{i+1}^{n+1} - u_{i-1}^{n+1}}{2\Delta x} \right) - \frac{(h_i^n)^3}{3} \left(\frac{u_{i+1}^{n+1} - 2u_i^{n+1} + u_{i-1}^{n+1}}{\Delta x^2} \right) = -Y_i^n \quad (\text{A.1})$$

458 and

$$459 \quad Y_i^n = 2\Delta t X_i^n - h_i^n u_i^{n-1} + (h_i^n)^2 \left(\frac{u_{i+1}^{n-1} - u_{i-1}^{n-1}}{2\Delta x} \right) + \frac{(h_i^n)^3}{3} \left(\frac{u_{i+1}^{n-1} - 2u_i^{n-1} + u_{i-1}^{n-1}}{\Delta x^2} \right).$$

461 Equation (A.1) can be rearranged into an explicit update scheme \mathcal{G}_u for u given its
 462 current and previous values, so that

$$463 \quad \begin{bmatrix} u_0^{n+1} \\ \vdots \\ u_m^{n+1} \end{bmatrix} = A^{-1} \begin{bmatrix} -Y_0^n \\ \vdots \\ -Y_m^n \end{bmatrix} =: \mathcal{G}_u(u^n, h^n, u^{n-1}, \Delta x, \Delta t) \quad (\text{A.2})$$

465 where A is a tri-diagonal matrix.

466 *Appendix A.2. Numerical Methods for Conservation of Mass Equation*

467 *Appendix A.2.1. \mathcal{E}_h*

468 The two step Lax-Wendroff update \mathcal{E}_h for h is

$$469 \quad h_{i+1/2}^{n+1/2} = \frac{1}{2} (h_{i+1}^n + h_i^n) - \frac{\Delta t}{2\Delta x} (u_{i+1}^n h_{i+1}^n - h_i^n u_i^n),$$

$$472 \quad h_{i-1/2}^{n+1/2} = \frac{1}{2} (h_i^n + h_{i-1}^n) - \frac{\Delta t}{2\Delta x} (u_i^n h_i^n - h_{i-1}^n u_{i-1}^n)$$

474 and

$$475 \quad h_i^{n+1} = h_i^n - \frac{\Delta t}{\Delta x} (u_{i+1/2}^{n+1/2} h_{i+1/2}^{n+1/2} - u_{i-1/2}^{n+1/2} h_{i-1/2}^{n+1/2}).$$

477 The quantities $u_{i\pm 1/2}^{n+1/2}$ are calculated using u^{n+1} obtained by applying \mathcal{G}_u (A.2) to u^n then
 478 linearly interpolating in space and time to give

$$479 \quad u_{i+1/2}^{n+1/2} = \frac{u_{i+1}^{n+1} + u_{i+1}^n + u_i^{n+1} + u_i^n}{4}$$

481 and

$$482 \quad u_{i-1/2}^{n+1/2} = \frac{u_i^{n+1} + u_i^n + u_{i-1}^{n+1} + u_{i-1}^n}{4}. \\ 483$$

484 Thus we have the following update scheme \mathcal{E}_h for (1a)

$$485 \quad \mathbf{h}^{n+1} = \mathcal{E}_h(\mathbf{u}^n, \mathbf{h}^n, \mathbf{u}^{n+1}, \Delta x, \Delta t). \quad (\text{A.3}) \\ 486$$

487 *Appendix A.2.2. \mathcal{G}_h*

488 The second order centered finite difference approximation to the conservation of
489 mass equation (1a) is

$$490 \quad h_i^{n+1} = h_i^{n-1} - \Delta t \left(u_i^n \frac{h_{i+1}^n - h_{i-1}^n}{\Delta x} + h_i^n \frac{u_{i+1}^n - u_{i-1}^n}{\Delta x} \right). \\ 491$$

492 Thus we have an update scheme \mathcal{G}_h for all i

$$493 \quad \mathbf{h}^{n+1} = \mathcal{G}_h(\mathbf{u}^n, \mathbf{h}^n, \mathbf{h}^{n-1}, \Delta x, \Delta t). \quad (\text{A.4}) \\ 494$$

495 *Appendix A.3. \mathcal{E}*

496 \mathcal{E} is the combination of (A.3) for (1a) and (A.2) for (1b) in the following way

$$497 \quad \begin{aligned} \mathbf{u}^{n+1} &= \mathcal{G}_u(\mathbf{u}^n, \mathbf{h}^n, \mathbf{u}^{n-1}, \Delta x, \Delta t) \\ \mathbf{h}^{n+1} &= \mathcal{E}_h(\mathbf{u}^n, \mathbf{h}^n, \mathbf{u}^{n+1}, \Delta x, \Delta t) \end{aligned} \quad \left\{ \mathcal{E}(\mathbf{u}^n, \mathbf{h}^n, \mathbf{u}^{n-1}, \mathbf{h}^{n-1}, \Delta x, \Delta t). \quad (\text{A.5}) \right. \\ 498$$

499 *Appendix A.4. \mathcal{G}*

500 \mathcal{G} is the combination of (A.4) for (1a) and (A.2) for (1b) in the following way

$$501 \quad \begin{aligned} \mathbf{h}^{n+1} &= \mathcal{G}_h(\mathbf{u}^n, \mathbf{h}^n, \mathbf{h}^{n-1}, \Delta x, \Delta t) \\ \mathbf{u}^{n+1} &= \mathcal{G}_u(\mathbf{u}^n, \mathbf{h}^n, \mathbf{u}^{n-1}, \Delta x, \Delta t) \end{aligned} \quad \left\{ \mathcal{G}(\mathbf{u}^n, \mathbf{h}^n, \mathbf{u}^{n-1}, \mathbf{h}^{n-1}, \Delta x, \Delta t). \quad (\text{A.6}) \right. \\ 502$$